Error reduction methods for integrated-path differential-absorption lidar measurements

Jeffrey R. Chen,[1,*] Kenji Numata,[1,2] and Stewart T. Wu[1]

[1]*NASA Goddard Space Flight Center, Greenbelt, Maryland, 20771, USA*
[2]*Department of Astronomy, University of Maryland, College Park, Maryland, 20742, USA*
[*] *jeffrey.r.chen@nasa.gov*

Abstract: We report new modeling and error reduction methods for differential-absorption optical-depth (DAOD) measurements of atmospheric constituents using direct-detection integrated-path differential-absorption lidars. Errors from laser frequency noise are quantified in terms of the line center fluctuation and spectral line shape of the laser pulses, revealing relationships verified experimentally. A significant DAOD bias is removed by introducing a correction factor. Errors from surface height and reflectance variations can be reduced to tolerable levels by incorporating altimetry knowledge and "log after averaging", or by pointing the laser and receiver to a fixed surface spot during each wavelength cycle to shorten the time of "averaging before log".

OCIS codes: (030.6600) Statistical optics; (280.1910) DIAL, differential absorption lidar; (120.0280) Remote sensing and sensors.

References and links

1. R. M. Measures, *Laser Remote Sensing: Fundamentals and Applications* (Wiley, 1984).
2. C. Weitkamp, *Lidar: Range Resolved Optical Remote Sensing of the Atmosphere* (Springer, 2005).
3. Space Studies Board, National Research Council, *Earth Science and Applications from Space: National Imperatives for the Next Decade and Beyond* (National Academies Press, 2007).
4. "A-SCOPE—advanced space carbon and climate observation of planet earth, report for assessment," ESA-SP1313/1(European Space Agency, 2008), *http://esamultimedia.esa.int/docs/SP1313-1_ASCOPE.pdf*.
5. G. Ehret, C. Kiemle, M. Wirth, A. Amediek, A. Fix, and S. Houweling, "Space-borne remote sensing of CO_2, CH_4, and N_2O by integrated path differential absorption lidar: a sensitivity analysis," Appl. Phys. B **90**(3-4), 593–608 (2008).
6. J. B. Abshire, H. Riris, G. Allan, X. Sun, S. R. Kawa, J. Mao, M. Stephen, E. Wilson, and M. A. Krainak, "Laser sounder for global measurement of CO_2 concentrations in the troposphere from space," in Laser Applications to Chemical, Security and Environmental Analysis, OSA Technical Digest (CD) (Optical Society of America, 2008), paper LMA4.
7. J. B. Abshire, H. Riris, G. R. Allan, C. J. Weaver, J. Mao, X. Sun, W. E. Hasselbrack, S. R. Kawa, and S. Biraud, "Pulsed airborne lidar measurements of atmospheric CO_2 column absorption," Tellus Ser. B, Chem. Phys. Meteorol. **62**(5), 770–783 (2010).
8. J. Caron and Y. Durand, "Operating wavelengths optimization for a spaceborne lidar measuring atmospheric CO_2.," Appl. Opt. **48**(28), 5413–5422 (2009).
9. M. J. T. Milton and P. T. Woods, "Pulse averaging methods for a laser remote monitoring system using atmospheric backscatter," Appl. Opt. **26**(13), 2598–2603 (1987).
10. A. Amediek, A. Fix, G. Ehret, J. Caron, and Y. Durand, "Airborne lidar reflectance measurements at 1.57 μm in support of the A-SCOPE mission for atmospheric CO_2," Atmos. Meas. Tech. **2**(2), 755–772 (2009).
11. J. Mao and S. R. Kawa, "Sensitivity studies for space-based measurement of atmospheric total column carbon dioxide by reflected sunlight," Appl. Opt. **43**(4), 914–927 (2004).
12. S. R. Kawa, J. Mao, J. B. Abshire, G. J. Collatz, X. Sun, and C. J. Weaver, "Simulation studies for a space-based CO_2 lidar mission," Tellus Ser. B, Chem. Phys. Meteorol. **62**(5), 759–769 (2010).
13. K. Numata, J. R. Chen, S. T. Wu, J. B. Abshire, and M. A. Krainak, "Frequency stabilization of distributed-feedback laser diodes at 1572 nm for lidar measurements of atmospheric carbon dioxide," Appl. Opt. **50**(7), 1047–1056 (2011).
14. F. Koyama and K. Oga, "Frequency chirping in external modulators," J. Lightwave Technol. **6**(1), 87–93 (1988).
15. J. Caron, Y. Durand, J. L. Bezy, and R. Meynart, "Performance modeling for A-SCOPE, a spaceborne lidar measuring atmospheric CO_2," Proc. SPIE **7479**, 74790E-1 (2009).
16. C. Stephan, M. Alpers, B. Millet, G. Ehret, P. Flamant, and C. Deniel, "MERLIN: a space-based methane monitor," Proc. SPIE **8159**, 815908, 815908–815915 (2011).
17. L. Mandel, "Interpretation of instantaneous frequency," Am. J. Phys. **42**(10), 840–846 (1974).

#162650 - $15.00 USD Received 14 Mar 2012; revised 25 May 2012; accepted 12 Jun 2012; published 26 Jun 2012

18. W. B. Grant, "Effect of differential spectral reflectance on DIAL measurements using topographic targets," Appl. Opt. **21**(13), 2390–2394 (1982).
19. J. W. Goodman, *Statistical Optics* (John Wiley & Sons, 1985).
20. N. Z. Hakim, B. E. A. Saleh, and M. C. Teich, "Generalized excess noise factor for avalanche photodiodes of arbitrary structure," IEEE Trans. Electron. Dev. **37**(3), 599–610 (1990).
21. J. D. Beck, R. Scritchfield, P. Mitra, W. Sullivan III, A. D. Gleckler, R. Strittmatter, and R. J. Martin, "Linear-mode photon counting with the noiseless gain HgCdTe e-APD," Proc. SPIE **8033**, 80330N, 80330N–15 (2011).
22. V. S. R. Gudimetla and M. J. Kavaya, "Special relativity corrections for space-based lidars," Appl. Opt. **38**(30), 6374–6382 (1999).
23. R. N. Clark, "Water frost and ice: the near-infrared spectral reflectance 0.65–2.5 μm," J. Geophys. Res. **86**(B4), 3087–3096 (1981).
24. M. Dumont, O. Brissaud, G. Picard, B. Schmitt, J. C. Gallet, and Y. Arnaud, "High-accuracy measurements of snow bidirectional reflectance distribution function at visible and NIR wavelengths – comparison with modeling results," Atmos. Chem. Phys. Discuss. **9**(5), 19279–19311 (2009).
25. D. S. Elliott, R. Roy, and S. J. Smith, "Extracavity laser band shape and bandwidth modification," Phys. Rev. A **26**(1), 12–18 (1982).
26. G. M. Stéphan, T. T. Tam, S. Blin, P. Besnard, and M. Têtu, "Laser line shape and spectral density of frequency noise," Phys. Rev. A **71**(4), 043809 (2005).
27. G. Di Domenico, S. Schilt, and P. Thomann, "Simple approach to the relation between laser frequency noise and laser line shape," Appl. Opt. **49**(25), 4801–4807 (2010).
28. N. A. Olsson, "Lightwave systems with optical amplifiers," J. Lightwave Technol. **7**(7), 1071–1082 (1989).
29. L. Mandel, "Fluctuations of photon beams: the distribution of the photo-electrons," Proc. Phys. Soc. **74**(3), 233–243 (1959).

1. Introduction

1.1 Overview

Lidar remote sensing techniques are powerful tools for global measurement of atmospheric constituents and parameters [1, 2]. The required precision and accuracy of such quantitative measurements have been increased to unprecedented levels for future airborne and space missions [3, 4]. To meet such stringent requirements, nadir-viewing, direct-detection, and pulsed integrated-path differential-absorption (IPDA) lidar techniques are being developed to measure the differential absorption optical depths (DAODs) of the target species in the column to the surface [5, 6]. From the DAOD and altimetry measurements and other ancillary data of the atmosphere (temperature, pressure, water vapor, etc.), the column number densities and dry mixing ratios of the target species can be retrieved [7, 8].

This paper addresses the following common issues with such DAOD measurements that have not been well addressed in previous publications: 1) error contribution from the optical frequency noise of a pulsed laser; 2) incorporation of a bias correction factor to reduce the averaging time for "log after averaging" (as named in [9]), and thereby minimize the impact of Etalon and atmospheric turbulence effects; 3) error contribution from the surface reflectance variations [10] when beam spots shift on the surface; 4) methods to reduce errors due to variations of surface height and reflectance; 5) estimation of the measurement precision of the transmitted laser pulse energy.

We present a statistical model to address these issues, to provide insight and estimation of DAOD measurement errors and to guide lidar system design and development. The model addresses both types of DAOD measurement errors: the relative random error (RRE) and the relative systematic error (RSE) (i.e., relative bias). This paper is organized as follows. After introducing several representative IPDA lidar examples in the next subsection, we quantify the error contributions from the laser frequency noise in section 2. In section 3, additional detection noise sources and a bias correction factor are incorporated into the model. A numerical example of the model is presented in section 4. The impact of surface reflectance variation is evaluated in section 5. A new method to reduce errors due to surface height variation is described in section 6. More considerations for the lidar system are discussed in section 7. Some supporting details are provided in the Appendix.

1.2 IPDA lidar examples

The Active Sensing of CO_2 Emissions over Nights, Days, and Seasons (ASCENDS) mission [3] has been planned by NASA to measure the global distribution of carbon dioxide (CO_2)

#162650 - $15.00 USD Received 14 Mar 2012; revised 25 May 2012; accepted 12 Jun 2012; published 26 Jun 2012

mixing ratios (~390 ppm in average) to ~1 ppm precision. A candidate IPDA lidar measurement approach for ASCENDS, being developed at NASA Goddard, allows simultaneous measurement of CO_2 and surface height in the same path [6, 7]. As shown in Fig. 1, a pulsed laser is wavelength-stepped across a single CO_2 line at 1572.335 nm [11] to measure the DAOD. To make the measurements uniformly sensitive to concentrations in the lower troposphere, the online wavelengths (ν_2 to ν_7) are placed at the sides of the line where the absorption is mostly from CO_2 molecules in the lower troposphere [12]. The two-way transmittance of the CO_2 line from a 400-km orbit (Fig. 1, *right*) has a narrow linewidth (~3.5 GHz) and steep slopes on the sides, making the measurements sensitive to laser frequency uncertainties. The offline points (ν_1 and ν_8) are placed in the adjacent window regions where the extremely low CO_2 absorption is essentially wavelength independent. To meet the mission end goal, the DAOD of the atmospheric CO_2 line needs to be measured with a RRE < 0.1% at multiple wavelengths across the absorption lines, and the variations of RSE need to be kept to a small fraction of the RRE. To reduce the RSE and RRE of the DAOD measurements, the detected photon count for each wavelength is averaged across multiple laser pulses before taking the logarithm of the on/off line ratio (i.e., "log after averaging"). This lidar approach will be used as a concrete example throughout this paper.

The partial RRE contribution from the laser frequency noise needs to be < 0.03%, to allow more margins for other error sources. In this paper, we show that the standard deviation of the effective laser frequency noise at online points for CO_2 needs to be < 0.23 MHz to meet this target. To satisfy such stringent requirements, laser pulses at each fixed wavelength are generally carved by amplitude modulating a frequency stabilized continuous-wave (CW) laser [13] (Fig. 1, *left*). The 1-μs wide pulses need to be at least ~100 μs apart, to completely clear the bottom ~15 km of the atmosphere, which eliminates crosstalk from cloud scattering. Chirp-free amplitude modulation [14] is used so that the laser pulses retain the instantaneous frequency of the CW laser.

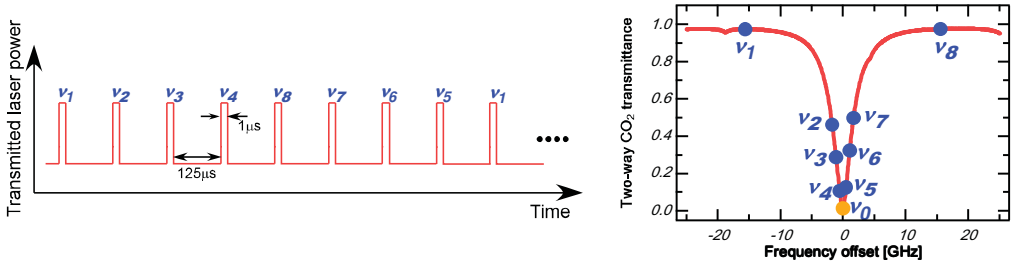

Fig. 1. The laser transmitter provides the wavelength-stepped pulse train (*left*) to repeatedly measure at 8 points across the 1572.335 nm CO_2 absorption line (*right*).

A similar CO_2 sounder space mission called A-SCOPE [4] has also been formulated by the European Space Agency. The A-SCOPE transmitter generates a pair of pulses, one at an online and the other at an offline wavelength, at an overall pulse pair repetition rate of 50 Hz, with a pulse energy of ~50 mJ. Comprehensive lidar sensitivity and spectroscopic analyses for the A-SCOPE instrument operating at either 1.57 μm or 2.05 μm CO_2 bands have been recently published [5, 8, 15]. A similar approach has been adopted for a planned methane sounder space mission dubbed MERLIN [16].

2. Measurement errors from laser frequency noise

Throughout this paper, $\bar{x}$ represents the ensemble average, $\sigma(x)$ the standard deviation, and $\sigma^2(x)$ the variance of x.

#162650 - $15.00 USD Received 14 Mar 2012; revised 25 May 2012; accepted 12 Jun 2012; published 26 Jun 2012

2.1 Treatment of laser frequency noise

The instantaneous frequency $\nu(t)$ of a single frequency CW laser can be modeled as an ergodic random process and the frequency noise is defined as $\delta_\nu(t) \equiv \nu(t) - \bar{\nu}$. The electric field of a pulse carved from the CW laser can be represented by the analytic signal of the CW laser field multiplied by the real single pulse amplitude $a(t-t_0)$ centered at time t_0, as given below

$$u(t) = a(t-t_0)\exp\Big(j[2\pi\bar{\nu}t + \phi(t)]\Big). \tag{1}$$

Here the instantaneous frequency is $\nu(t) = \bar{\nu} + (1/2\pi)\,d\phi/dt$. The single-sided energy spectral density (ESD) of $u(t)$, denoted as $L(\nu_F)$ as a function of the Fourier frequency ν_F, represents a short-term spectrum of the CW laser within a pulse duration Δt. The line-center frequency $\nu_c(t_0)$ of $L(\nu_F)$ is linked to the instantaneous frequency $\nu(t)$ and $a(t)$ [17] as

$$\nu_c(t_0) \equiv \int_0^\infty \nu_F L_N(\nu_F)d\nu_F = \int_{-\infty}^{\infty} \nu(t)h(t-t_0)dt. \tag{2}$$

Here $L_N(\nu_F) \equiv L(\nu_F)\Big/\int_0^\infty L(\nu_F)d\nu_F$ and $h(t) \equiv a^2(t)\Big/\int_{-\infty}^{\infty} a^2(t)dt$ are the normalized ESD of $u(t)$ and normalized pulse intensity envelope, respectively. As to be seen in this subsection and in Appendix A, the laser frequency noise contributes to measurement errors through two complimentary factors, the line shape $L(\nu_F)$ and the fluctuation of the line-center frequency $\nu_c(t_0)$. Both factors are jointly determined by the frequency noise and pulse amplitude $a(t)$.

As shown in Eq. (2), the fluctuation of the line-center frequency $\delta_{\nu 1}(t_0) \equiv \nu_c(t_0) - \bar{\nu}$ is an average of the CW laser frequency noise $\delta_\nu(t)$ within a pulse duration Δt weighted by $h(t-t_0)$. For a top-hat pulse shape, $\delta_{\nu 1}(t_0)$ is simply a running average of $\delta_\nu(t)$ within Δt. The variance $\sigma^2(\delta_{\nu 1})$ of $\delta_{\nu 1}(t_0)$ can be obtained by integrating its power spectral density (PSD), which in turn can be derived from $S_{\delta\nu}(f)$, the PSD of $\delta_\nu(t)$. Since $\delta_{\nu 1}(t_0)$ is a correlation between $\delta_\nu(t)$ and $h(t)$ as seen in Eq. (2), its PSD $S_{\delta\nu 1}(f)$ is related to $S_{\delta\nu}(f)$ by

$$S_{\delta\nu 1}(f) = S_{\delta\nu}(f)\big|H(f)\big|^2, \tag{3}$$

where $H(f)$ is the Fourier transform of $h(t)$. As the ESD of $h(t)$, $|H(f)|^2$ serves as a window function to filter the frequency noise represented by $S_{\delta\nu}(f)$. For a top-hat $h(t) = \mathrm{rect}(t/\Delta t)/\Delta t$, the corresponding window function becomes $|H(f)|^2 = \mathrm{sinc}^2(f\Delta t)$. Fast frequency noise components above its effective bandwidth $1/\Delta t$ are quickly averaged out as noise frequency f increases. As shown in subsection 2.5, this has been verified experimentally with the seed laser described in [13].

Formulation linking $L(\nu_F)$ to the frequency noise $S_{\delta\nu}(f)$ and the pulse amplitude $a(t)$ is further derived and discussed in Appendix A. Interestingly, the remaining frequency noise that is filtered out by $|H(f)|^2$ contributes to the bandwidth of the line shape $L(\nu_F)$.

2.2 Single pulse formulation

The energy absorption of a single laser pulse through a thin layer of target molecules is given by

#162650 - $15.00 USD Received 14 Mar 2012; revised 25 May 2012; accepted 12 Jun 2012; published 26 Jun 2012

$$dL(\nu_F, l) = -L(\nu_F, l)\sigma_0(\nu_F, l)N(l)dl. \tag{4}$$

Here $\sigma_0(\nu_F, l)$ is the absorption cross-section of the molecules at Fourier frequency ν_F and path length l, and $N(l)$ is the number density of the molecules at path length l. The laser pulse energy $E(l)$ at a path length l can be obtained from Eq. (4) as

$$\begin{aligned} E(l) &= E(0)\exp\left[-\tau(\nu_c, l)\right], \\ \tau(\nu_c, l) &\equiv \int_0^l \sigma_{eff}(\nu_c, l')N(l')dl'. \end{aligned} \tag{5}$$

Here $\tau(\nu_c, l)$ is the effective optical depth of the species of interest and $\sigma_{eff}(\nu_c, l)$ is the effective absorption cross-section defined as

$$\begin{aligned} \sigma_{eff}(\nu_c, l) &\equiv \int_0^\infty \sigma_0(\nu_F, l)L_N(\nu_F, l)d\nu_F = \frac{\int_0^\infty \sigma_0(\nu_F, l)T(\nu_F, l)L(\nu_F, 0)d\nu_F}{\int_0^\infty T(\nu_F, l)L(\nu_F, 0)d\nu_F}, \\ T(\nu_F, l) &\equiv \exp\left[-\tau_0(\nu_F, l)\right], \\ \tau_0(\nu_F, l) &\equiv \int_0^l \sigma_0(\nu_F, l')N(l')dl'. \end{aligned} \tag{6}$$

Here $\tau_0(\nu_F, l)$ is the monochromatic optical depth of the species of interest, and other attenuation factors are assumed to be wavelength independent.

To account for two-way absorption, the path length l is taken to be the accumulated distance that the laser pulse has traveled, running from 0 to $2r_G$ as the laser pulse travels from the spacecraft to the surface (outgoing path) and back to the spacecraft (return path). Here r_G is the distance from the spacecraft to the surface. Our model uses the effective optical depth to include the line shape factor, which causes only a bias $\tau(\nu_c, l) - \tau_0(\nu_c, l)$ to the optical depth. As shown in Appendix A, this bias can be accurately corrected. When $L(\nu_F)$ is much narrower than the spectral width of the target absorption line, this bias even becomes negligible, as shown in subsection 2.6 for the 1572.335 nm CO_2 line. When $L(\nu_F)$ is broad, the one-way effective optical depth may no longer be the same for the outgoing and return paths so that $\tau(\nu_c, 2r_G) = 2\tau(\nu_c, r_G)$ may become invalid (see Appendix A for more details).

Incorporating other attenuation factors [18], the detected laser pulse energy W_s backscattered from the surface becomes

$$W_s = E_s A_s \exp\left[-\tau(\nu_c, 2r_G)\right], \tag{7}$$

where E_s is the transmitted laser pulse energy, $A_s \equiv \rho T_{atm}^2 D / r_G^2$ is the lump sum of attenuation factors excluding $\exp[-\tau(\nu_c, 2r_G)]$, D is a instrument constant, ρ is the ground surface reflectance (in sr^{-1}), and T_{atm} is the one-way transmittance of the atmosphere excluding the target species.

The lidar receiver can operate in either linear mode with an internal gain or photon counting mode. To cover both cases, the analog detector signal and noise are gain normalized and expressed in detected photon count K. For any type of radiation (including thermal light), the ensemble average and the variance of K and the optical energy W entering the detector area are related by [19, 20]

$$\overline{K} = \alpha\overline{W}, \tag{8}$$

$$\sigma^2(K) = F_e\overline{K} + \alpha^2\sigma^2(W). \tag{9}$$

#162650 - $15.00 USD Received 14 Mar 2012; revised 25 May 2012; accepted 12 Jun 2012; published 26 Jun 2012

Here $\alpha \equiv \eta / (h\bar{\nu})$ is proportional to the detector quantum efficiency η, and h is the Planck constant. Note that only the shot noise contribution is multiplied by the detector's excess noise factor F_e. To estimate errors, we expand $\exp[-\tau(\nu_c, 2r_G)]$ in Eq. (7) around $\bar{\nu}$ to arrive at

$$W_s = E_s A_s \exp\left[-\tau(\bar{\nu}, 2r_G)\right]\left[1-(d\tau / d\nu_c)\delta_{\nu 1}(t_0) + b\delta_{\nu 1}{}^2(t_0)\right], \tag{10}$$

where $b \equiv [(d\tau / d\nu_c)^2 - d^2\tau / d\nu_c^2] / 2$. From Eqs. (8) and (10), the ensemble mean of the detected signal photon count K_s is

$$\overline{K_s} = \alpha \overline{W_s} = \alpha E_s A_s \exp\left[-\tau(\bar{\nu}, 2r_G)\right]\left[1 + b\sigma^2(\delta_{\nu 1})\right], \tag{11}$$

where the variance $\sigma^2(\delta_{\nu 1})$ of $\delta_{\nu 1}(t_0)$ contributes a small fractional bias $b\sigma^2(\delta_{\nu 1})$ to $\overline{K_s}$. As illustrated in subsection 2.6, this bias is usually negligible in practice. Using Eqs. (9) and (10), the variance of K_s is related to the laser line-center frequency noise as

$$\sigma^2(K_s) = F_e \overline{K_s} + \alpha^2 \sigma^2(W_s) = F_e \overline{K_s} + \left(\overline{K_s}\right)^2 \left(d\tau / d\nu_c\right)^2 \sigma^2(\delta_{\nu 1}), \tag{12}$$

where the small contribution from the quadratic term $b\delta_{\nu 1}{}^2(t_0)$ is neglected.

2.3 Averaging across multiple pulses

We now turn to estimate the two-way DAOD $\Delta\tau \equiv \tau(\bar{\nu}_{on}, 2r_G) - \tau(\bar{\nu}_{off}, 2r_G)$ between online and offline laser frequencies $\bar{\nu}_{on}$ and $\bar{\nu}_{off}$. Up to section 6, $\tau(\nu_c, 2r_G)$ is assumed to be constant over the path and duration of the multiple pulses to be averaged. Although the measurement of E_s is affected by the amplified spontaneous emission (ASE) in the laser amplifiers, the resulting measurement errors are negligible in practice and thus will not be included in the present model (see Appendix B for details).

For each online or offline wavelength, the laser pulses are assumed to have the same $h(t)$ and a period of t_p. From Eq. (10), the following sum of normalized pulse energies (SNE) can be introduced to include the effect of the laser frequency noise

$$\begin{aligned} S_{NE1} &\equiv \sum_{i=0}^{n-1} \frac{W_s(i)}{E_s(i)} = \exp\left[-\tau(\bar{\nu}, 2r_G)\right]\left(\sum_{i=0}^{n-1} A_s(i)\right)\left[1 - \frac{d\tau}{d\nu_c}\delta_{\nu n}(t) + bQ_n(t)\right], \\ Q_n(t) &\equiv \frac{1}{\sum_{i=0}^{n-1} A_s(i)} \sum_{i=0}^{n-1}\left[A_s(i)\delta_{\nu 1}{}^2(t + i \times t_p)\right], \end{aligned} \tag{13}$$

where the averaged laser line-center frequency noise $\delta_{\nu n}(t)$ across n pulses $(i = 0, 1, 2, .., n-1)$ is given by

$$\delta_{\nu n}(t) \equiv \frac{1}{\sum_{i=0}^{n-1} A_s(i)} \sum_{i=0}^{n-1}\left[A_s(i)\delta_{\nu 1}(t + i \times t_p)\right]. \tag{14}$$

The mean and variance of S_{NE1} are found to be

$$\overline{S_{NE1}} = \exp\left[-\tau(\bar{\nu}, 2r_G)\right]\left(\sum_{i=0}^{n-1} A_s(i)\right)\left(1 + b\sigma^2(\delta_{\nu 1})\right), \tag{15}$$

$$\sigma^2(S_{NE1}) = \left(\overline{S_{NE1}}\right)^2 \left(d\tau / d\nu_c\right)^2 \sigma^2(\delta_{\nu n}). \tag{16}$$

#162650 - $15.00 USD Received 14 Mar 2012; revised 25 May 2012; accepted 12 Jun 2012; published 26 Jun 2012

Superscripts (or subscripts) *on* and *off* will be used to indicate online and offline laser frequencies, respectively. The offline $\sigma^2(S_{NE1}^{off})$ can be neglected because of the negligible slope $(d\tau/d\nu_c)_{off}$.

Corresponding to S_{NE1}, the sum of normalized photon count K_s (SNK) is defined as $S_{NK1} \equiv \sum_{i=0}^{n-1} K_s(i)/E_s(i)$ and its mean is found to be $\overline{S_{NK1}} = \alpha \overline{S_{NE1}}$. Here S_{NK1} is named with the following scheme. *S* stands for sum, *NK* for normalized photon count, and the trailing digit 1 is used to distinguish S_{NK1} from S_{NK2} and S_{NK3} to be introduced in sections 3 and 6, respectively. Using $\overline{K_s(i)K_s(i')} = \alpha^2 \overline{W_s(i)W_s(i')}$ [19], the variance of S_{NK1} is found to be

$$\begin{aligned} \sigma^2(S_{NK1}) &= F_e \overline{S_{NNK1}} + \alpha^2 \sigma^2(S_{NE1}), \\ S_{NNK1} &\equiv \sum_{i=0}^{n-1} \frac{K_s(i)}{E_s^{\,2}(i)} \cong S_{NK1}/E_{sav} \cong S_K/E_{sav}^2. \end{aligned} \tag{17}$$

Here S_{NNK1} is named similarly, with *NN* indicating that K_s is normalized twice. The integrated photon count S_K and average transmitted pulse energy E_{sav} are defined as $S_K \equiv \sum_{i=0}^{n-1} K_s(i)$ and $E_{sav} \equiv \left(\sum_{i=0}^{n-1} E_s(i)\right)/n$, respectively. S_{NNK1} is essentially S_K normalized by E_{sav}^2. The first term in $\sigma^2(S_{NK1})$ stems from the shot noise. The second term arises solely from the laser line-center frequency noise.

From Eq. (15), $\Delta\tau$ is related to S_{NK1} by

$$\Delta\tau = -\ln\left(\frac{\overline{S_{NK1}^{on}}}{\overline{S_{NK1}^{off}}}\right) + \ln(R_A) + \ln(R_b), \tag{18}$$

where $R_A \equiv \sum_{i=0}^{n-1} A_s^{on}(i) / \sum_{i=0}^{n-1} A_s^{off}(i) \equiv 1 + \delta_{RA}$ and $R_b \equiv [1 + b^{on}\sigma^2(\delta_{\nu 1}^{on})]/[1 + b^{off}\sigma^2(\delta_{\nu 1}^{off})]$. For the rest of this paper, we assume the transmitted pulse energies are approximately the same for online and offline pulses so that $\overline{S_K^{on}} \cong \overline{S_K^{off}} \exp(-\Delta\tau)$. $\Delta\tau$ has been in effect estimated from the following "log after averaging" estimator [5–9]

$$\Delta\tau_{SNK1} \equiv -\ln\left(\frac{S_{NK1}^{on}}{S_{NK1}^{off}}\right). \tag{19}$$

To estimate errors, approximations $\overline{\ln(x)} \cong \ln\left(\bar{x}\right) - (1/2)\sigma^2(x)/\left(\bar{x}\right)^2$ (accurate to the third order) and $\sigma^2\left(\ln(x)\right) \cong \sigma^2(x)/\left(\bar{x}\right)^2$ (accurate to the second order) are used in our calculations. The bias $b_{\Delta\tau\_SNK1} \equiv \overline{\Delta\tau_{SNK1}} - \Delta\tau$ and variance of $\Delta\tau_{SNK1}$ are found to be

$$b_{\Delta\tau\_SNK1} \cong -\ln(R_A) - \ln(R_b) + \frac{F_e}{2}\left(\frac{\overline{S_{NNK1}^{on}}}{\overline{S_{NK1}^{on}}^2} - \frac{\overline{S_{NNK1}^{off}}}{\overline{S_{NK1}^{off}}^2}\right) + \frac{1}{2}\left(\frac{d\tau}{d\nu_c}\right)_{on}^2 \sigma^2(\delta_{\nu n}^{on}), \tag{20}$$

$$\sigma^2(\Delta\tau_{SNK1}) \cong \frac{\sigma^2(S_{NK1}^{on})}{\overline{S_{NK1}^{on}}^2} + \frac{\sigma^2(S_{NK1}^{off})}{\overline{S_{NK1}^{off}}^2} \cong \frac{F_e}{\overline{S_K^{off}}}[1 + \exp(\Delta\tau)] + \left(\frac{d\tau}{d\nu_c}\right)_{on}^2 \sigma^2(\delta_{\nu n}^{on}). \tag{21}$$

#162650 - $15.00 USD Received 14 Mar 2012; revised 25 May 2012; accepted 12 Jun 2012; published 26 Jun 2012

As expected, the shot noise contribution to $\sigma^2(\Delta\tau_{SNK1})$ is inversely proportional to the integrated photon count $\overline{S_K}$. However, it is important to use S_{NK1} rather than S_K to estimate $\Delta\tau$, to remove the effect of variation in $E_s(i)$. The laser line-center frequency noise contribution to the DAOD RRE is $[(d\tau/d\nu_c)_{on}/\Delta\tau]\sigma(\delta_{vn}^{on})$, where $\sigma(\delta_{vn}^{on})$ is the standard deviation of the averaged line-center frequency noise of the on-line laser (averaged across n pulses). It becomes clear that $\delta_{vn}^{on}(t)$ represents the effective frequency noise. Obviously, an on-line laser frequency bias $\Delta\bar{\nu}_{on}$ will result in a DAOD bias $\sim(d\tau/d\nu_c)_{on}\Delta\bar{\nu}_{on}$ [5]. This bias can be avoided by accurate calibration and thus is neglected throughout this paper.

2.4 Frequency noise reduction from pulse averaging

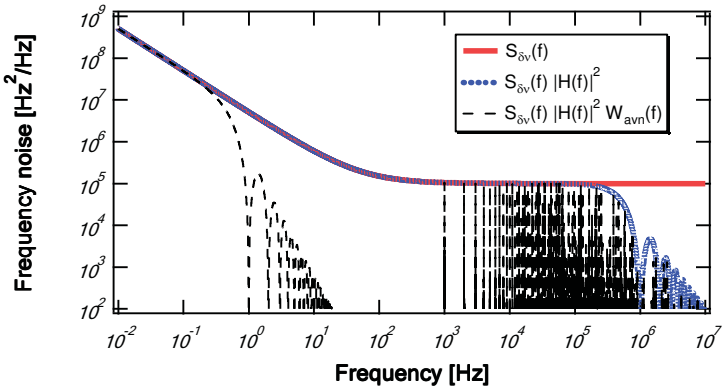

Fig. 2. The nominal laser frequency noise PSD $S_{\delta\nu}(f)=h_{-1}/f+h_0$ (solid red) is suppressed to $S_{\delta\nu}(f)|H(f)|^2$ (dotted blue) by averaging within a 1-μs top-hat pulse and further reduced to $S_{\delta\nu}(f)|H(f)|^2W_{avn}(f)$ (dashed black) by averaging across 1000 identical pulses separated by a period of 1 ms.

We now turn to link the PSD $S_{\delta vn}(f)$ of $\delta_{vn}(t)$ to $S_{\delta\nu}(f)$. From Eq. (14) we have

$$S_{\delta vn}(f)=S_{\delta\nu}(f)|H(f)|^2W_{avn}(f),$$
$$W_{avn}(f)\equiv\left|\frac{1}{\sum_{i=0}^{n-1}A_s(i)}\sum_{i=0}^{n-1}A_s(i)\exp(j2\pi ft_p\times i)\right|^2. \tag{22}$$

Here the effect of multiple-pulse averaging on the PSD is an additional multiplicative window function $W_{avn}(f)$. The overall window function $|H(f)|^2W_{avn}(f)$ is the ESD of the weighted pulse train function $\sum_{i=0}^{n-1}\left[A_s(i)h(t-i\times t_p)\right]/\sum_{i=0}^{n-1}A_s(i)$. $W_{avn}(f)$ is a periodic function with a period equal to the pulse repetition rate. Using the orthogonal property of the phase shift factor $\exp(j2\pi ft_p\times i)$, its averaged height is found to be

$$<W_{avn}>=\sum_{i=0}^{n-1}A_s^2(i)/\left(\sum_{i=0}^{n-1}A_s(i)\right)^2. \tag{23}$$

When the weighting factors $A_s(i)$ are the same, $W_{avn}(f)$ becomes $\mathrm{sinc}^2(nft_p)/\mathrm{sinc}^2(ft_p)$ with an average height of $1/n$. This is consistent with n-fold variance reduction when averaging n identical but uncorrelated random variables. As shown in section 5, $<W_{avn}>$ is

#162650 - $15.00 USD Received 14 Mar 2012; revised 25 May 2012; accepted 12 Jun 2012; published 26 Jun 2012

only slightly higher than 1/*n* when measured surface reflectance data are used for $A_s(i)$, and will be taken to be 1/*n* for our numerical evaluations.

The present model reveals relationships not available from previous models [5, 8]. Using Eq. (22), the effective frequency noise can be estimated in terms of $S_{\delta\nu}(f)$, as illustrated in Fig. 2 for a representative frequency stabilized seeder laser. The nominal $S_{\delta\nu}(f)$ can be approximated by $S_{\delta\nu}(f) = h_{-1}/f + h_0$, where constant h_{-1} and h_0 quantify flicker noise and a nearly flat noise floor for f above 100 Hz, respectively. The periodical window function $W_{avn}(f)$ suppresses the frequency noise except in its narrow peaks at $f = m_w / t_p$ ($m_w = 0, 1, 2, 3, ...$). Frequency drifts with periods longer than the averaging time fall in the window peak at $f = 0$ and thus are not attenuated from this averaging. Since the PSD is nearly constant over the frequency range of all other window peaks ($m_w = 1, 2, 3, ...$), the variance of the faster frequency noise components (excluding the slow drifts) is essentially reduced by a factor of *n*. This frequency noise reduction has also been verified experimentally, as shown in the next subsection.

2.5 Experimental results

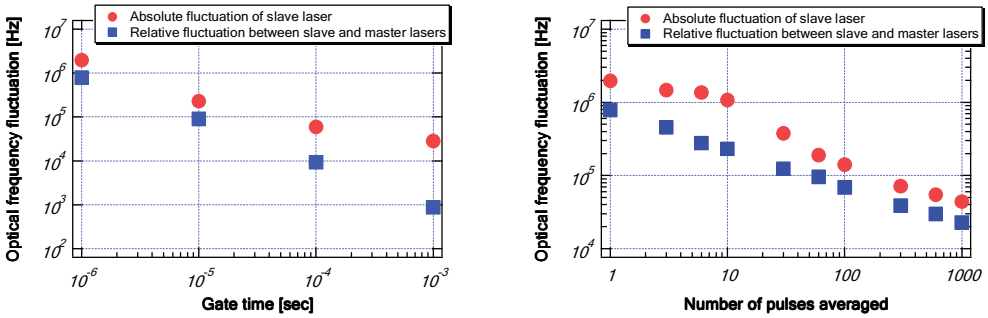

Fig. 3. (*left*) The standard deviation of the absolute frequency of the slave laser and frequency offset between the slave and master lasers measured within a gating time from 1 μs to 1 ms; (*right*) Both frequencies were also measured periodically within a 1-μs gating time with a 1-ms period and averaged across multiple measurements. The standard deviation of each averaged frequency, computed from 100 averaged samples, is plotted as a function of the number of measurements being averaged.

Equations (3) and (22) have been verified experimentally with our seed laser described in [13]. Figure 3 (*left*) shows the standard deviation of the absolute frequency of the slave laser and frequency offset between the slave and master lasers measured within a gating time from 1 μs to 1 ms. The absolute frequency noise was measured from the beatnote between two identical and independent laser units. The noise of the frequency offset was measured from the beatnote between the slave and master lasers. A fast frequency counter (HP 5371A, Agilent Technologies, Inc.) was used to measure the beatnote frequencies. The measured noise decreases as the gating time increases, matching the reducing area under $S_{\delta\nu}(f)|H(f)|^2$.

Both frequencies were also measured periodically within a 1-μs gating time with a 1-ms period and averaged across multiple measurements. The standard deviation of each averaged frequency, computed from 100 averaged samples, is plotted in Fig. 3 (*right*) as a function of *n*, the number of measurements being averaged. The variance of the averaged frequency decreases as *n* increases, matching the reducing area under $S_{\delta\nu}(f)|H(f)|^2 W_{avn}(f)$.

2.6 Frequency stability requirements for ASCENDS

Using Eqs. (5) and (6), the relative error $(\Delta\tau - \Delta\tau_0)/\Delta\tau_0$ due to the finite line shape $L(\nu_F)$ is numerically evaluated and shown in Fig. 4(*left*) as functions of the effective bandwidth 1/Δ*t*

#162650 - $15.00 USD Received 14 Mar 2012; revised 25 May 2012; accepted 12 Jun 2012; published 26 Jun 2012

of a top-hat laser pulse shape for the CO_2 line. As detailed in Appendix A, the line shape $L(\nu_F)$ is simply taken to be the ESD of the top-hat pulse shape. $(\Delta\tau - \Delta\tau_0)/\Delta\tau_0$ is smaller than a 0.02% target [5] and thus does not need to be corrected for all three online points (with frequency offsets + 0.5 GHz, + 1.1 GHz, and + 1.7 GHz) when the pulsewidth Δt is longer than 0.5 μs. τ is taken to be the same as τ_0 for the CO_2 line in our numerical examples where Δt is assumed to be ~1 μs.

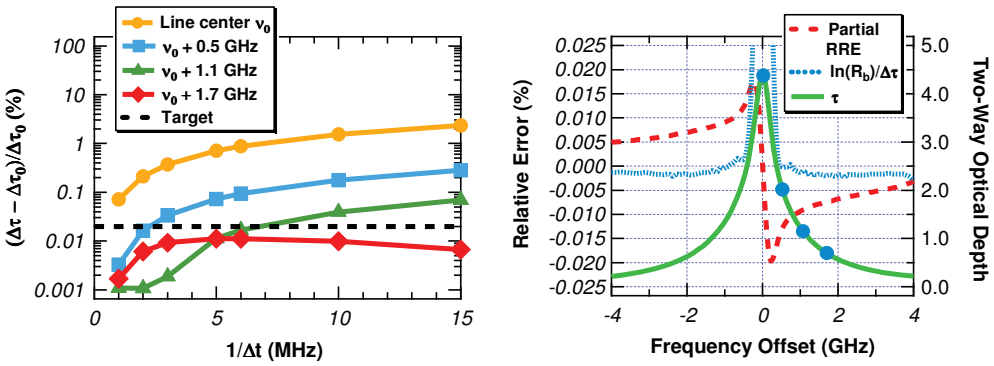

Fig. 4. Relative errors for atmospheric CO_2 DAOD measurements: (*left*) $(\Delta\tau - \Delta\tau_0)/\Delta\tau_0$ due to the finite linewidth $1/\Delta t$ of a top-hat pulse shape (calculated from Eqs. (5) and (6)); (*right*) laser line-center frequency noise contributions to the RRE for $\sigma(\delta_{vn}^{on}) = 0.1$ MHz (dashed red, calculated from Eq. (21)), and RSE $\ln(R_b)/\Delta\tau$ for $\sigma(\delta_{v1}) = 10$ MHz (dotted blue, from Eq. (18)) as functions of the online laser frequency offset from the absorption line center. The two-way optical depth τ (solid green) is also plotted, with blue dots marking the same online and absorption line-center frequency points used on the left.

Table 1. RRE Targets, Relevant Parameters, and Resulting Effective Laser Frequency Noise Requirement for Atmospheric CO_2 DAOD Measurement

Requirement	Value	Parameter	Value
Budget for total RRE $\sigma(\Delta\tau)/\Delta\tau$	0.1%	$\tau(\nu_c, 2r_G)$ online (typical)	~2.0
Budget for partial RRE from laser frequency noise	0.03%	$\tau(\nu_c, 2r_G)$ offline (15.6 GHz laser frequency offset)	0.013
Upper bound of $\sigma(\delta_{vn}^{on})$ (0.5 GHz laser frequency offset)	0.23 MHz	Sensitivity of RRE to $\sigma(\delta_{vn}^{on})$ (0.5 GHz frequency offset)	0.13% /MHz

The partial RRE $[(d\tau/d\nu_c)_{on}/\Delta\tau]\sigma(\delta_{vn}^{on})$ for $\sigma(\delta_{vn}^{on}) = 0.1$ MHz, the partial RSE $|\ln(R_b)|/\Delta\tau$, and $\tau(\nu_c, 2r_G)$ are plotted in Fig. 4(*right*) for atmospheric CO_2, as functions of the online laser frequency offset from the absorption line center. Table 1 summarizes the RRE targets, relevant parameters, and resulting effective laser frequency noise requirement for atmospheric CO_2 DAOD measurement. The frequency offset of the offline laser is set at 15.6 GHz. To bound the RRE to < 0.03% for an online frequency ≥ 0.5 GHz away from the absorption line center, the standard deviation $\sigma(\delta_{vn}^{on})$ of the effective frequency noise needs to be suppressed down to 0.23 MHz. This frequency stability requirement has been satisfied experimentally (see [13] and subsection 2.5).

The partial RSE $|\ln(R_b)|/\Delta\tau$ for $\sigma(\delta_{v1}) = 10$ MHz is less than 0.002% at such online frequencies, and thus negligible. However, this bias and $(\Delta\tau - \Delta\tau_0)/\Delta\tau_0$ (Fig. 4, *left*) become significant near the absorption line center, where the excessive CO_2 absorption also results in higher RRE. It is thus undesirable to place an online frequency point near the absorption line center. Referring to Eq. (20), the last bias term $(d\tau/d\nu_c)_{on}^2\sigma^2(\delta_{vn}^{on})/2$ is $< 10^{-7}$ when $[(d\tau/d\nu_c)_{on}/\Delta\tau]\sigma(\delta_{vn}^{on})$ is bound to 0.03%, and thus negligible. The third bias term can be reduced to a negligible level with photon count integration. As shown in section

#162650 - $15.00 USD Received 14 Mar 2012; revised 25 May 2012; accepted 12 Jun 2012; published 26 Jun 2012

5, the remaining bias term $|\ln(R_A)|$ can be reduced to $<1.1\times10^{-4}$. Overall, the RSE $b_{\Delta\tau\_SNK1}/\Delta\tau$ can be reduced to $< 0.02\%$.

3. Incorporating additional detection noise sources

We now incorporate additional detection noise sources arising from the background solar radiation, detector dark count, and receiver circuitry noise for the lidar receiver. The mean and variance of the photon count $K_{n\text{-}n}$ produced by the background solar radiation is given by $\overline{K_{n-n}} = 2\alpha N_{bgd} B_o \Delta t$ and $\sigma^2(K_{n-n}) = F_e \overline{K_{n-n}}$, where $2N_{bgd}$ is the PSD of the background solar radiation and B_o the optical filter bandwidth. The equivalent detector dark count K_d (normalized by the mean internal gain M_e of the detector) has a mean and variance given by $\overline{K_d} = \lambda_d \Delta t$ and $\sigma^2(K_d) = F_d \overline{K_d}$, where λ_d is an equivalent dark count rate and F_d an effective dark-count excess noise factor. The equivalent photon count K_T arising from the receiver circuitry noise has a zero mean and a variance $\sigma^2(K_T)$ given by

$$\begin{aligned} &\sigma^2(K_T) = I_{\delta i}\Delta t / \left(M_e e\right)^2, \\ &I_{\delta i} \equiv \int_{-\infty}^{\infty} S_{\delta i}(f)\,\mathrm{sinc}^2(f\Delta t)\Delta t df, \end{aligned} \tag{24}$$

where $S_{\delta i}(f)$ is the PSD of the equivalent input noise current of the circuit and e the electron charge. Equation (24) is derived by the same steps leading to Eq. (40) for $\sigma^2(K_{s-n})$ (see Appendix B). The integration $I_{\delta i}$ can be approximated by $S_{\delta i}(0)$ when the detector electrical bandwidth B_e is much larger than $1/\Delta t$.

The laser signal photon count K_s is estimated as $K'_s = K_{tot} - K'_{bgd}$, where K_{tot} is the total count $K_{tot} = K_s + K_{n-n} + K_d + K_T$ measured within Δt, and $K'_{bgd} = K'_{n-n} + K'_d + K'_T$ is the background count within Δt scaled from a separate measurement taken between the pulse measurements. This background measurement can be taken in a longer duration $\beta\Delta t$, where β is a background integration time multiplier, to reduce the background variance. Obviously, $\overline{K'_s} = \overline{K_s}$. Referencing Eq. (9), the variance of K'_s is found to be

$$\begin{aligned} &\sigma^2(K'_s) \equiv F_e \overline{K_s} + \alpha^2\sigma^2(W_s) + \lambda_{bgd}\Delta t, \\ &\lambda_{bgd} \equiv \left[2\alpha N_{bgd} B_o F_e + F_d\lambda_d + I_{\delta i}/\left(M_e e\right)^2\right]\left(1+1/\beta\right). \end{aligned} \tag{25}$$

The transmitted pulse energy E_s can be estimated as $E'_s = E'_{tot} - E'_{bgd}$ where E_{tot} is the total detected energy and the background energy E'_{bgd} arises from the circuitry noise, dark current in the detector, and ASE in the laser amplifiers. The mean of E'_s equals E_s and the variance of E'_s can be neglected (see Appendix B). The additional noise sources can be included by replacing S_{NK1} with $S_{NK2} \equiv \sum_{i=0}^{n-1} K'_s(i)/E'_s(i)$. Similarly, S_K is replaced by $S_{K'} \equiv \sum_{i=0}^{n-1} K'_s(i)$. Obviously, $\overline{S_{NK2}} = \overline{S_{NK1}}$. The normalized variance of S_{NK2} is found to be

$$\frac{\sigma^2(S_{NK2})}{\left(\overline{S_{NK2}}\right)^2} \cong F_e \frac{\overline{S_{NNK2}}}{\left(\overline{S_{NK2}}\right)^2} + \left(\frac{d\tau}{d\nu_c}\right)^2 \sigma^2(\delta_{vn}) + \frac{\overline{S_{NN2}}}{\left(\overline{S_{NK2}}\right)^2}\lambda_{bgd}\Delta t, \tag{26}$$

where S_{NNK2} and S_{NN2} are defined as $S_{NNK2} \equiv \sum_{i=0}^{n-1} K'_s(i)/E'^2_s(i)$ and $S_{NN2} \equiv \sum_{i=0}^{n-1} 1/E'^2_s(i)$. Here S_{NN2} is named similarly, with *NN* indicating double normalization.

#162650 - $15.00 USD Received 14 Mar 2012; revised 25 May 2012; accepted 12 Jun 2012; published 26 Jun 2012

As seen from Eq. (20), the "log after averaging" DAOD estimator in Eq. (19) leads to an additive bias term $(1/2)F_e(\overline{S_{NNK1}^{on}}/\overline{S_{NK1}^{on}}^2 - \overline{S_{NNK1}^{off}}/\overline{S_{NK1}^{off}}^2) \cong (1/2)F_e/\overline{S_K^{on}}$, and thus requires significant photon count integration ($\overline{S_K^{on}} \sim 10^4$) to bring the bias term down to a tolerable level ($\sim 10^{-4}$). When using S_{NK2}, the additional background variance $\lambda_{bgd}\Delta t$ in $\sigma^2(K'_s)$ results in an additional DAOD bias term $(1/2)\lambda_{bgd}\Delta t(\overline{S_{NN2}^{on}}/\overline{S_{NK2}^{on}}^2 - \overline{S_{NN2}^{off}}/\overline{S_{NK2}^{off}}^2)$. These two bias terms can be reduced significantly by incorporating the following bias correction factor $C_{\Delta\tau\_SNK2}$ into the DAOD estimator given below

$$\begin{aligned}
&\Delta\tau_{SNK2} \equiv -\ln\left(\frac{S_{NK2}^{on}}{S_{NK2}^{off}}\right) + C_{\Delta\tau_SNK2},\\
&C_{\Delta\tau_SNK2} \equiv \frac{F_e}{2}\left(\frac{S_{NNK2}^{off}}{{S_{NK2}^{off}}^2} - \frac{S_{NNK2}^{on}}{{S_{NK2}^{on}}^2}\right) + \frac{\lambda_{bgd}\Delta t}{2}\left(\frac{S_{NN2}^{off}}{{S_{NK2}^{off}}^2} - \frac{S_{NN2}^{on}}{{S_{NK2}^{on}}^2}\right).
\end{aligned} \tag{27}$$

As shown next, the sum of the two bias terms is reduced from $\sim (1/2)F_e/\overline{S_{K'}^{on}}$ to $\sim (1/2)F_e^2/\overline{S_{K'}^{on}}^2$ by the bias correction factor $C_{\Delta\tau\_SNK2}$. The residual bias $\sim (1/2)F_e^2/\overline{S_{K'}^{on}}^2$ becomes tolerable ($\sim 10^{-4}$) even when the integrated photon count $\overline{S_{K'}^{on}}$ is as low as ~100. Such a low photon count $\overline{S_{K'}^{on}}$ can be obtained within a few pulses, or even within a single pulse without averaging.

Using the bias-corrected DAOD estimator $\Delta\tau_{SNK2}$ given by Eq. (27), the bias $b_{\Delta\tau\_SNK2} \equiv \overline{\Delta\tau_{SNK2}} - \Delta\tau$ and variance of $\Delta\tau_{SNK2}$ are found to be

$$\begin{aligned}
&b_{\Delta\tau_SNK2} \cong -\ln(R_A) - \ln(R_b) + \left(d\tau/d\nu_c\right)_{on}^2 \sigma^2(\delta_{vn}^{on})/2 + b_{C_\Delta\tau_SNK2},\\
&b_{C_\Delta\tau_SNK2} \equiv -\frac{1}{2}\left(F_e/\overline{S_{K'}^{on}}\right)^2\left[1-\exp(-2\Delta\tau)\right] - \frac{3}{2}F_e n\lambda_{bgd}\Delta t\left[1-\exp(-3\Delta\tau)\right]/\overline{S_{K'}^{on}}^3,
\end{aligned} \tag{28}$$

$$\begin{aligned}
&\sigma^2(\Delta\tau_{SNK2}) \cong \sigma_{\Delta\tau DET}^2 + \left(d\tau/d\nu_c\right)_{on}^2 \sigma^2(\delta_{vn}^{on}),\\
&\sigma_{\Delta\tau DET}^2 \equiv F_e[1+\exp(\Delta\tau)]/\overline{S_{K'}^{off}} + n\lambda_{bgd}\Delta t[1+\exp(2\Delta\tau)]/\overline{S_{K'}^{off}}^2.
\end{aligned} \tag{29}$$

It should be noted that all the parameters in the bias correction factor $C_{\Delta\tau\_SNK2}$ are measureable. For example, the background variance $\lambda_{bgd}\Delta t$ can be measured when the laser pulses are off. However, it may not be feasible to measure some of the parameters (such as F_e) constantly during the flight. Consequently, long-term variations of such parameters may degrade the bias correction.

To minimize the time-varying Etalon and atmospheric turbulence effects, it is desirable to reduce n, the number of pulses being averaged for $\Delta\tau_{SNK2}$. To do this, the overall averaging time T_{tot} is divided into m slots (each is T_{tot}/m long), and a $\Delta\tau_{SNK2}$ (denoted as $\Delta\tau_{SNK2}(k)$) is evaluated within each slot $(k = 0, 1, 2, .., m-1)$. $\Delta\tau$ can then be estimated from the average of $\Delta\tau_{SNK2}(k)$ given below

$$\Delta\tau_{SNK2\_av} \equiv \frac{1}{m}\sum_{k=0}^{m-1}\Delta\tau_{SNK2}(k). \tag{30}$$

#162650 - $15.00 USD Received 14 Mar 2012; revised 25 May 2012; accepted 12 Jun 2012; published 26 Jun 2012

The variance of $\Delta\tau_{SNK2\_av}$ (excluding contribution from the slow laser frequency drifts) also decreases approximately by the number of participating pulses (i.e., $n \times m$), as in the case for $\Delta\tau_{SNK2}$. However, the averaging in Eq. (30) cannot effectively reduce the bias to $\Delta\tau$.

4. Numerical estimation of measurement errors

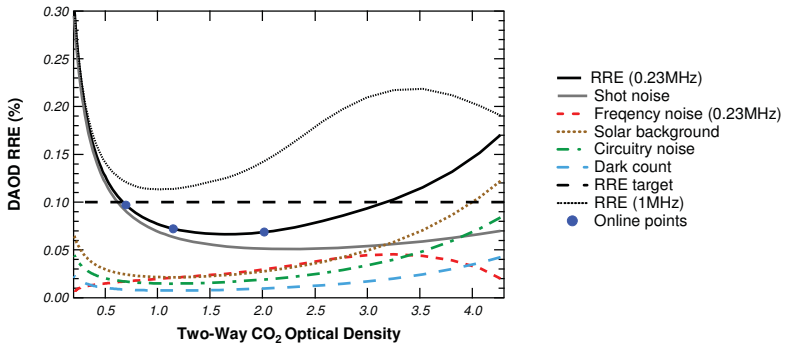

Fig. 5. The RRE $\sigma(\Delta\tau_{SNK2\_av})$ /$\Delta\tau$ for atmospheric CO_2 DAOD measurement (solid black) as a function of the two-way optical depth, computed from Eqs. (29) and (30) using parameters listed in Table 2. The blue dots mark the three online frequency points used in Fig. 4. Also plotted are partial contributions to this RRE from the shot noise (solid grey), frequency noise (dashed red), solar background (dotted brown), receiver circuitry noise (dash-dotted green), and detector dark count (long-dashed blue). The standard deviation of the effective frequency noise $\sigma(\delta_{vn}^{on})$ averaged in 10 s is 0.23 MHz for the above calculations. When it is increased to 1 MHz, the RRE (dotted black) rises above the 0.1% target (dashed black).

Using realistic parameters listed in Table 2, $\Delta\tau_{SNK2\_av}$ / $\Delta\tau$, the RRE for atmospheric CO_2 DAOD measurement, is computed and plotted as a function of τ in Fig. 5. Partial contributions to the RRE from the signal shot noise ~ $F_e[1+\exp(\Delta\tau)]/\overline{S_{K'}^{off}}$, frequency noise, solar background, receiver circuitry noise, and detector dark count are also shown Fig. 5. When there are 3200 detected photons (in average) for each offline pulse, the RRE is ≤ 0.1% for τ between 0.66 and 3.2. This photon count can be achieved with $E_s = 4$ mJ for an average ρ = 0.17. The detector specifications listed in Table 2 can be met with a state-of-the-art HgCdTe avalanche photodiode (APD) detector [21]. The detected solar radiation count $K_{n\text{-}n}$ is estimated for a zenith angle of 75°. Its noise contribution is larger than that from the receiver transimpedance amplifier (TIA). The noise from the dark count K_d is negligible. It should be noted that the RRE increases sharply when the online point moves further away from the line center, confining the frequency offset of the online points to within ± 1.7 GHz from the CO_2 absorption line center. The standard deviation of the effective frequency noise averaged in the 10-s measurement time is taken to be 0.23 MHz for the above calculations. When it is increased to 1 MHz, the RRE rises above the 0.1% target (also shown in Fig. 5).

#162650 - $15.00 USD Received 14 Mar 2012; revised 25 May 2012; accepted 12 Jun 2012; published 26 Jun 2012

Table 2. Parameters Used to Evaluate the RRE of Δτ as a Function of τ

Parameter	Value	Parameter	Value
Operating wavelength	1572 nm	Detector output dark current i_d	1 nA
Orbit altitude	400 km	Single-sided TIA equivalent input noise current	1 pA/Hz$^{1/2}$
Telescope diameter	1.5 m	B_e (electrical bandwidth)	1.6 MHz
Receiver field of view (full angle)	150 μrad	B_o (optical bandwidth)	48 GHz
Beam spot diameter on surface	50 m	Background solar photon count rate $K_{n-n}/\Delta t$	129 MHz
T_{atm} (one-way transmittance of atmosphere excluding CO_2)	0.7	β (background integration time multiplier)	10
ρ (surface reflectance)	0.17 sr^{-1}	Δt (pulse duration)	1 μs
Receiver path transmittance	0.51	E_s (transmitted pulse energy)	4 mJ
A_s (see Eq. (7))	1.48x10^{-13}	K_s (signal photon count)	3200
η (detector quantum efficiency)	70%	T_{tot} (overall averaging time)	10 s
M_e (detector internal gain)	400	m (see Eq. (30))	10
F_e (excess noise factor)	2	effective n in T_{tot}/m	500
F_d (dark-count excess noise factor)	2	$\sigma(\delta_{vn}^{on})$ averaged in T_{tot}	0.23 MHz

It is desirable to squeeze down RRE contributions from noise sources other than the signal shot noise. This will translate into reduction in required laser power and hence the cost. The laser peak power entering the lidar receiver needs to be high enough so that the signal shot noise contribution is well above the noise contributions from the receiver circuitry and the solar background count. This is the case for Goddard's ASCENDS lidar where online points are placed at least 0.4 GHz away from the CO_2 line center with $\tau \le 2.4$.

5. Impact of surface reflectance variation

Table 3. Parameters Used for Evaluation of the Impact of Surface Reflectance Variation

Parameter	Value	Parameter	Value
Speed of spacecraft	7 km/s	Pulse rate for each channel	1 kHz
Beam spot diameter on surface	50 m	Pulse duration	1 μs
Number of wavelength channels	8	Duration of averaging	1 s
Combined pulse rate	8 kHz	Path length within averaging time	7 km

As discussed earlier, the surface reflectance variation adds a bias $|\ln(R_A)|$ to the DAOD estimation. Since this bias varies from one path to another, it needs to be kept to a small fraction of the 0.1% RRE. Also, the PSD of the effective laser frequency noise $\delta_{vn}(t)$ is reduced by the periodical window function W_{avn} whose average height $< W_{avn} >$ depends on the variation of $A_s(i)$. Both factors are quantified here using measured surface reflectance data in [10] for realistic error estimation.

#162650 - $15.00 USD Received 14 Mar 2012; revised 25 May 2012; accepted 12 Jun 2012; published 26 Jun 2012

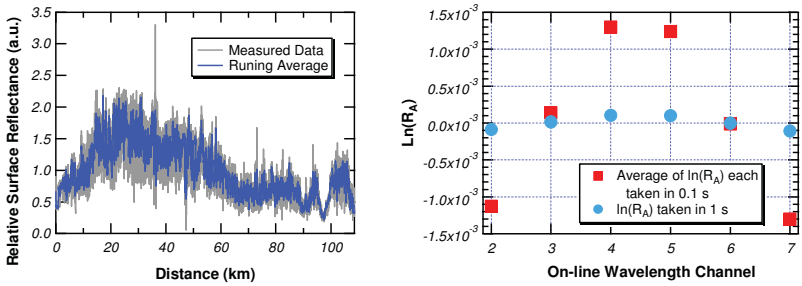

Fig. 6. (*left*) Relative surface reflectance: measured data (grey) and its running average over a length of 50 m (blue), courtesy of A. Amediek of Deutsches Zentrum für Luft- und Raumfahrt (DLR); (*right*) $\ln(R_A)$ calculated from surface reflectance data for the worst case. For each online wavelength channel, two $\ln(R_A)$ are calculated from both offline sum $\sum_{i=0}^{n-1} A_s^{off}(i)$ for 1-s averaging time and the average is plotted (blue dot). An average of 10 consecutive $\ln(R_A)$ values, each computed as above over 0.1 s averaging time, is also plotted (red square).

The parameters used for the evaluation are listed in Table 3. The laser beam is assumed to travel at the same speed as the spacecraft. As shown in Fig. 1, the laser pulses are assumed to repeatedly cycle through wavelength channels 1, 2, 3, 4, 8, 7, 6, 5, 1, to minimize the separation between online (channels 2 to 6) and offline (channels 1 and 8) pulses. A set of surface reflectance data that has strong variations is used for this evaluation. The surface reflectance measurement was taken in southern Spain using ~10-m laser spot size and a step size of ~6 m [10]. To convert this data to the reflectance for our beam size, a 1-D running average is taken within our beam size (50 m) and the averaged reflectance is used as $A_s(i)$ in our calculation. The raw and averaged reflectance data are plotted in Fig. 6 (*left*). For an averaging time of 1 s, there are n = 1000 pulses for each wavelength and the path length is 7 km. In contrast, the separation between online and offline beam spots is only 2.1 m at most. Consequently, the ratio R_A is very close to 1. This point is confirmed by our calculation results shown in Fig. 6 (*right*). The 108-km total path length is divided into 15 sections (7 km each) and $\ln(R_A)$ is evaluated for each section. For each online wavelength channel, its starting pulse for sum $\sum_{i=0}^{n-1} A_s^{on}(i)$ comes in between two adjacent offline pulses, each serves as the starting pulse for its offline sum $\sum_{i=0}^{n-1} A_s^{off}(i)$. Each $\sum_{i=0}^{n-1} A_s^{off}(i)$ is used to calculate $\ln(R_A)$ and the average of the two is plotted in Fig. 6 (*right*) for the worst case where the bias $|\ln(R_A)|$ is $< 1.1\times10^{-4}$. The corresponding RSE is smaller than 0.02% if the two-way DAOD is kept > 0.55.

$|\ln(R_A)|$ is increased when the averaging time (hence n) is reduced. Figure 6 (*right*) also shows an average of 10 values of $\ln(R_A)$, each computed as above over 0.1 s averaging time consecutively along the worst path. For some wavelength channels, this averaged bias $|\ln(R_A)|$ becomes larger than 10^{-3} and thus unacceptable. To reduce the bias $|\ln(R_A)|$, it is crucial to allow a fast pulse repletion rate (≥ 1 kHz for each wavelength) and a sufficient integration time (≥ 1 s), and to properly interleave online and offline pulses to minimize their separation.

The average height $< W_{avn} >$ of $W_{avn}(f)$ is also evaluated for the 7-km averaging paths. The calculated $< W_{avn} >$ is quite close to 1/n, varying between 1.01/n and 1.12/n.

#162650 - $15.00 USD Received 14 Mar 2012; revised 25 May 2012; accepted 12 Jun 2012; published 26 Jun 2012

6. Mitigating impact of surface height variation

The DAOD errors due to surface height variation can be reduced to negligible levels if pulse-by-pulse knowledge of surface height is incorporated into the formulation. Let $z_0(i)$ be the surface height at laser beam spot *i* relative to a certain reference ground surface, and $z(i)$ a measured value of $z_0(i)$. r_G now represents the range from the spacecraft to the reference surface. The distance from the spacecraft to the actual surface is $r_G - z_0(i)$. Since $z_0(i)$ could vary by tens of meters over the path of pulse averaging, $\tau(r_G - z_0(i))$ could fluctuate over a few tenths of a percent over the path, resulting in additional DAOD errors. To mitigate this problem, we estimate $\Delta\tau(2r_G)$ (i.e., the two-way DAOD from the spacecraft to the reference surface and back to the spacecraft) from $S_{NK3} \equiv \sum_{i=0}^{n-1} K'_s(i) / [A_z(i)E'_s(i)]$, where $A_z(i) \equiv \exp[2\sigma_{eff}(\bar{\nu}, r_G)N(r_G)z(i)]$ is introduced to account for the fluctuation of the optical depth. The corresponding estimator $\Delta\tau_{SNK3}$ of $\Delta\tau(2r_G)$ can be easily adapted from $\Delta\tau_{SNK2}$ in Eq. (27) by simply replacing $E'_s(i)$ with $A_z(i)E'_s(i)$ in the relevant terms in $\Delta\tau_{SNK2}$ (i.e., S_{NK2}, S_{NNK2}, and S_{NN2}). As shown next, the variation of the surface height $z_0(i)$ does not affect such estimation of $\Delta\tau(2r_G)$. Nevertheless, the imperfect measurement of $z_0(i)$ still leads to additional DAOD errors.

To simplify the treatment, we assume $z(i) = z_0(i) + \Delta z + \delta_z(i)$, where Δz represents a slowly varying altimetry bias, and $\delta_z(i)$ a zero-mean random altimetry error. Δz is treated as a constant during the *n* pulse averaging, and the $\delta_z(i)$ values among different pulses are assumed to be uncorrelated and have the same variance σ_z^2. Expanding $1/A_z(i)$ in S_{NK3} as

$$1/A_z(i) \equiv \exp(-2\sigma_{eff}N\Delta z) / \exp[2\sigma_{eff}Nz_0(i)]\left(1 - 2\sigma_{eff}N\delta_z(i) + 2[\sigma_{eff}N\delta_z(i)]^2\right), \quad (31)$$

the bias $b_{\Delta\tau\_SNK3} \equiv \overline{\Delta\tau_{SNK3}} - \Delta\tau(2r_G)$ and variance of $\Delta\tau_{SNK3}$ are found to be

$$\begin{aligned} &b_{\Delta\tau\_SNK3} = b_{\Delta\tau\_SNK2} + b_{\Delta\tau z}, \\ &b_{\Delta\tau z} \equiv 2\sigma_{eff}(\bar{\nu}_{on}, r_G)N(r_G)\Delta z - 2\left[\sigma_{eff}(\bar{\nu}_{on}, r_G)N(r_G)\sigma_z\right]^2 (1 - < W_{avn} >), \end{aligned} \quad (32)$$

$$\begin{aligned} &\sigma^2(\Delta\tau_{SNK3}) = \sigma^2(\Delta\tau_{SNK2}) + \sigma^2_{\Delta\tau z}, \\ &\sigma^2_{\Delta\tau z} \equiv \left[2\sigma_{eff}(\bar{\nu}_{on}, r_G)N(r_G)\sigma_z\right]^2 < W_{avn} >. \end{aligned} \quad (33)$$

Here we have neglected $\sigma_{eff}(\bar{\nu}_{off}, r_G)$ that is much smaller than $\sigma_{eff}(\bar{\nu}_{on}, r_G)$. The additional DAOD bias $b_{\Delta\tau z}$ arises from the altimetry bias Δz as well as the variance σ_z^2. The additional DAOD variance $\sigma^2_{\Delta\tau z}$ scales with the altimetry variance σ_z^2 and $< W_{avn} >$, decreasing with ~1/*n*. Taking atmospheric CO_2 for example, an altimetry precision $\sigma_z = 20$ m results in $\sigma_{eff}(\bar{\nu}_{on}, r_G)N(r_G)(20\text{m}) < 15\times10^{-4}$, leading to a negligible standard deviation $\sigma_{\Delta\tau z} < 1.3\times10^{-4}$ (assuming *n* = 500), and a negligible DAOD bias ($< 1.4\times10^{-6}$) arising from σ_z^2. On the other hand, the altimetry bias Δz needs to be kept below 0.66 m to limit its DAOD bias contribution to $< 10^{-4}$.

#162650 - $15.00 USD Received 14 Mar 2012; revised 25 May 2012; accepted 12 Jun 2012; published 26 Jun 2012

7. Discussions

7.1 Other error sources

Other DAOD measurement error sources have also been studied previously [5–8, 15, 16]. An important one is the time-varying Etalon fringes in the lidar's frequency response. It is crucial to minimize multi-path interference (MPI) along the optical train, and to shorten the time of "averaging before log", to minimize the impact of the Etalon effect. Using multiple wavelength channels also helps to correct for the Etalon effect. The wavelength dependency of the lidar's spectral response in the receiving path can be partially removed by passing a small fraction of the transmitted laser trough the receiving path and measuring the transmitted pulse energy E'_s at the end of the path [15]. Another error in the measurement of K'_s arises from the broadening of the returned signal pulses mainly due to the structured ground surface. The spectral crosstalk among multiple wavelength channels must be suppressed to maintain spectral purity for the measurement [5].

The contribution of atmospheric turbulence to the bias term $|\ln(R_A)|$ is negligible because T_{atm} essentially does not change during the time separation between an online pulse and either of its neighboring offline pulses (< 0.4 ms). The speckle noise can be also neglected in direct detection IPDA lidar instruments with a telescope diameter of ~1.5 m and laser beam spot size of ~50 m on the surface [5, 7]. The Doppler effect can be either made negligible or corrected for practical nadir viewing IPDA lidars [15, 22]. The Doppler shift due to high speed cross-wind [15] can be made negligible by minimizing the off-nadir angle of the laser beam. The 2° off-nadir angle intended for A-SCOPE lidar to avoid detector saturation from the ice cloud glint [15] appears to be unnecessary because the reflectance of the ice (and snow) is particularly small for both 1.57 μm and 2.05 μm wavelength regions [23, 24]. The Doppler shift deduced from the spacecraft velocity components can also be compensated by dynamically shifting the frequency offset of the seed laser [13]. The laser beam divergence (~ ± 62.5 μrad) in Table 2 results in a continuous spread of laser frequency of ± 278 kHz across the beam at 1570 nm [15]. Since this small spread is deterministic and symmetrical, it does not increase the variance of $\Delta\tau$ and its bias contribution to $\Delta\tau$ is negligible.

7.2 Error reduction tradeoffs

When the laser peak power entering the lidar receiver is high enough so that the signal shot noise contribution is well above the noise contributions from the receiver circuitry and the background count, the ratio η / F_e of the detector becomes a figure of merit for the DAOD measurement. For a fixed average power, further increasing the laser peak power by reducing the pulsewidth or the pulse repetition rate will no longer reduce $\sigma^2_{\Delta\tau DET}$ effectively. On the other hand, it is desirable to use the maximum pulse repetition rate (~10 kHz for all wavelengths combined) to reduce the bias $|\ln(R_A)|$, and to use a wider pulsewidth (along with the high pulse repetition rate) to reduce $\sigma^2(\delta_{vn})$ and the laser peak power. The laser peak power must be kept below the threshold of the undesirable stimulated Brillouin scattering (SBS) in the laser power amplifiers. The pulsewidth, repetition rate and laser peak power chosen for Goddard's ASCENDS approach appear to be appropriate. Using a shorter pulse duration (< 100 ns) and a lower pulse repetition rate results in less frequency noise reduction, and may thus require a seed laser with a narrower frequency noise bandwidth and a lower noise floor.

7.3 Shortening the time of averaging before log

As shown earlier, all DAOD bias terms other than $|\ln(R_A)|$ can potentially be reduced to negligible levels by averaging across just a few pulses (or even without averaging) before log. It would be great if the same can be done for the bias term $|\ln(R_A)|$, to reduce the time of averaging before log. This could be achieved by pointing the laser and receiver to a fixed

#162650 - $15.00 USD Received 14 Mar 2012; revised 25 May 2012; accepted 12 Jun 2012; published 26 Jun 2012

surface spot during each wavelength sweep cycle (≤ 1 ms). During such a short time, the slow spacecraft pointing jitter can be ignored. As long as the online/offline laser spots coincide within each wavelength sweep, slow pointing jitters do not increase $|\ln(R_A)|$. The pointing can be achieved, for example, with piezoelectrically driven steering mirrors. While the spacecraft is traveling, the laser and receiver can be pointed to a fixed surface point for several online/offline cycles and then quickly redirected to the next fixed surface point. The mirror steering span can be reduced to only one or two beam spots to allow fast redirection. Even for a long pointing duration of 1 s, the fractional change in path length is less than 4×10^{-5} and thus negligible.

With this pointing scheme, the overall time of averaging before log can be significantly shortened to reduce measurement errors as mentioned earlier. On the other hand, using pointing mechanism may complicate the instrument design and pose a reliability challenge.

8. Summary

New modeling and error reduction methods are presented for DAOD measurements of atmospheric constituents using direct-detection IPDA lidars. Errors from the laser frequency noise are quantified in terms of the line center fluctuation and spectral line shape of the laser pulses, revealing new relationships that have been verified experimentally. Averaging across *n* pulses, the effective frequency noise is quantified by the multiplicative window function that filters the PSD of the instantaneous frequency noise. This in general leads to *n*-fold reduction in the variance of the effective frequency noise (excluding slow drifts with periods longer than the measurement averaging time). To bound the frequency noise contribution to the DAOD RRE to 0.03%, the standard deviation of the effective frequency noise needs to be < 0.23 MHz for ASCENDS' CO_2 transmitter.

The DAOD variance decreases approximately by the number of participating pulses. A significant DAOD bias can be essentially canceled out by incorporating a correction factor. The RRE and RSE of the DAOD due to surface height and reflectance variations can be reduced to tolerable levels by incorporating pulse-by-pulse altimetry knowledge and by "log after averaging", or by pointing the laser and receiver to a fixed surface spot during each wavelength sweep to shorten the time of averaging before log.

The predominant errors in the transmitted pulse energy measurement are found to be negligible in practice. Error reduction tradeoffs are investigated and illustrated with realistic calculations that take various detection noise sources into account. Other error sources are also summarized.

Appendix

A. Formulation linking $L(\nu_F)$ to $S_{\delta\nu}(f)$ and $a(t)$

The bandwidth B_L of $L(\nu_F)$, as defined below, is also linked to $v(t)$ and $a(t)$ [17] as

$$
\begin{aligned}
B_L{}^2 &\equiv \int_0^\infty \left[\nu_F - \nu_c(t_0)\right]^2 L_N(\nu_F)\,d\nu_F = B_{LF}{}^2 + B_{LA}{}^2,\\
B_{LF}{}^2 &\equiv \int_{-\infty}^{\infty} \left[\nu(t) - \nu_c(t_0)\right]^2 h(t-t_0)\,dt,\\
B_{LA}{}^2 &\equiv \frac{\int_{-\infty}^{\infty} f^2\,|A(f)|^2\,df}{\int_{-\infty}^{\infty} |A(f)|^2\,df} = \frac{1}{4\pi^2}\,\frac{\int_{-\infty}^{\infty}\left[da(t)/dt\right]^2 dt}{\int_{-\infty}^{\infty} a^2(t)\,dt}.
\end{aligned}
\tag{34}
$$

Here $A(f)$ is the Fourier transform of $a(t)$ so that $|A(f)|^2$ is the ESD of $a(t)$.

As seen from Eq. (34), B_L^2 is the sum of two components. The first component $B_{LF}{}^2$ is the time domain "variance" of $\delta_{\nu 0} \equiv \nu(t) - \nu_c(t_0)$ weighted by $h(t-t_0)$, and the second

#162650 - $15.00 USD Received 14 Mar 2012; revised 25 May 2012; accepted 12 Jun 2012; published 26 Jun 2012

component $B_{LA}{}^2$ represents the bandwidth of $|A(f)|^2$ arising from the variations of the amplitude envelope $a(t)$. From Eq. (34), the ensemble average of $B_{LF}{}^2$ is found to be

$$\overline{B_{LF}{}^2} = \overline{[\delta_\nu(t)]^2} - \overline{[\delta_{\nu 1}(t_0)]^2} = \int_{-\infty}^{\infty} S_{\delta\nu}(f)\left[1 - |H(f)|^2\right] df . \quad (35)$$

This shows that $\overline{B_{LF}{}^2}$ arises from faster frequency noise components, excluding the slower components $S_{\delta\nu}(f)|H(f)|^2$ that determine the line center fluctuation. Since the contributing fast frequency noise components are quite repeatable from one pulse duration to another, $B_{LF}{}^2$ has little fluctuation around its ensemble mean $\overline{B_{LF}{}^2}$ and thus causes little variance in $b_\tau(\nu_c, l) \equiv \tau(\nu_c, l) - \tau_0(\nu_c, l)$. In practice, the frequency noise PSD $S_{\delta\nu}(f)$ cuts off eventually, resulting in a finite $\overline{B_{LF}{}^2}$ [17]. Since the slow frequency drifts do not contribute, $\overline{B_{LF}{}^2}$ for a short pulse can be significantly smaller than that for the underlying CW laser.

To facilitate further analysis, we rewrite $L(\nu_F)$ as $L_0(\Delta\nu_F) \equiv L(\nu_c(t_0) + \Delta\nu_F)$, as a function of the Fourier frequency offset $\Delta\nu_F \equiv \nu_F - \nu_c(t_0)$. Obviously, a broad $|A(f)|^2$ (due to, for example, a narrow pulsewidth) can still lead to a significant bias $b_\tau(\nu_c, l)$. Fortunately, the bias $b_\tau(\nu_c, l)$ can be computed from Eqs. (5) and (6) using $L_0(\Delta\nu_F) = |A(\Delta\nu_F)|^2$ when the frequency noise contribution is negligible. Equations (5) and (6) thus allow accurate modeling even when $L(\nu_F)$ is deterministically broadened to suppress SBS in the laser amplifiers. Since the amplitude modulation is deterministic, the bias $b_\tau(\nu_c, l)$ is deterministic and thus can be precisely calibrated and removed. Although $L(\nu_F)$ for a top hat pulse shape has an infinite B_{LA}, the relative error $(\Delta\tau - \Delta\tau_0)/\Delta\tau_0$ can still be negligible as shown in Fig. 4 (*left*). When $L(\nu_F)$ is broad, the one-way effective optical depth may no longer be the same for the outgoing and return paths. This is due to the progressive distortion of the laser line shape $L_N(\nu_F, l)$ caused by the absorption of the species of interest. Since the laser line shape $L_N(\nu_F, l)$ is no longer the same along the two paths, $\sigma_{eff}(\nu_c, l)$ may have two different values for each spatial position, one for the outgoing laser pulse and the other for the return laser pulse.

The relationship between the CW laser line shape PSD and the frequency noise PSD $S_{\delta\nu}(f)$ has been established in previous studies [25–27]. The present work further links $L(\nu_F)$, the laser pulse ESD, to $S_{\delta\nu}(f)$ and the pulse shape $a(t)$. $L(\nu_F)$ is the Fourier transform of the following autocorrelation of $u(t)$

$$R_u(t_D) \equiv \int_{-\infty}^{\infty} u^*(t)u(t + t_D)dt = \int_{-\infty}^{\infty} a(t')a(t' + t_D)\exp(j2\pi\bar{\nu}t_D)\exp(j\Delta\phi)dt', \quad (36)$$

where $t' \equiv t - t_0$ and $\Delta\phi \equiv \phi(t' + t_0 + t_D) - \phi(t' + t_0)$. The ensemble average of $L_0(\Delta\nu_F)$ becomes

$$\overline{L_0(\Delta\nu_F)} = \int_{-\infty}^{\infty}\left[\int_{-\infty}^{\infty} a(t')a(t' + t_D)\overline{\exp\left(j[\Delta\phi - 2\pi\delta_{\nu 1}(t_0)t_D]\right)}dt'\right]\exp(-j2\pi\Delta\nu_F t_D)dt_D . \quad (37)$$

Since $\Delta\phi - 2\pi\delta_{\nu 1}(t_0)t_D$ is a zero-mean Gaussian process, we have

$$\overline{\exp\left(j[\Delta\phi - 2\pi\delta_{\nu 1}(t_0)t_D]\right)} = \exp\left[-\frac{1}{2}\overline{\left(\Delta\phi - 2\pi\delta_{\nu 1}(t_0)t_D\right)^2}\right]. \quad (38)$$

#162650 - $15.00 USD Received 14 Mar 2012; revised 25 May 2012; accepted 12 Jun 2012; published 26 Jun 2012

Using $\Delta\phi = \int_{t'+t_0}^{t'+t_0+t_D} \delta v(t)dt$ and taking similar steps as in [25, 26], we finally arrive at

$$\overline{L_0(\Delta\nu_F)} = \int_{-\infty}^{\infty} R_0(t_D)\exp(-j2\pi\Delta\nu_F t_D)dt_D,$$
$$R_0(t_D) \equiv \int_{-\infty}^{\infty} a(t')a(t'+t_D)\exp\left[-2\pi^2 t_D{}^2 \int_{-\infty}^{\infty} S_{\delta\nu}(f)\left|\mathrm{sinc}(ft_D) - H(f)\exp\left[j2\pi f\left(t'+t_D/2\right)\right]\right|^2 df\right]dt'. \quad (39)$$

The phase factor $\exp\left[j2\pi f\left(t'+t_D/2\right)\right]$ in $R_0(t_D)$ stems from the time delay between $\Delta\phi$ (centered at $t'+t_D/2+t_0$) and $\delta_{v1}(t_0)$ (centered at t_0). Following the argument in [17] leading to Eq. (34), one arrives at $\overline{B_L^2} = -(1/2\pi)^2(d^2R_0/dt_D^2)_{t_D=0}/R_0(0)$ that yields $\overline{B_L^2} = B_{LA}^2 + \overline{B_{LF}^2}$, the same result as given by Eqs. (34) and (35). The corresponding formula for CW laser [25] is a limiting case of Eq. (39) when $a(t)$ is taken to be a constant. Similar to the CW formula, Eq. (39) in general leads to a non-analytical line shape $\overline{L_0(\Delta\nu_F)}$ that can only be computed numerically.

B. Impact of transmitted laser pulse energy measurement errors

We now evaluate the DAOD errors arising from the transmitted laser pulse energy measurement errors. We assume that the laser amplifier ASE received by the detector has a uniform optical power spectral density of $2N_{ASE}$ (N_{ASE} for each polarization) within an optical bandwidth B_o, and the laser is polarized and has a detected power of P_s during Δt. For ease of analysis, we further assume that both the laser and ASE received by the detector are uniformly distributed among N_{MM} spatial modes and the electrical-field product of any two different spatial modes does not contribute to the detector current (due to mode orthogonality). The detected photon rate then becomes $\lambda(t) = \alpha[P_s + P_{n-n} + P_{s-n}]$ where $P_{n-n}(t)$ is the ASE power, $P_{s-n}(t)$ corresponds to the product of the laser electrical field and the ASE electrical field (referred to as s-n beat term). $\alpha P_{s-n}(t)$ has a zero mean and double-sided PSD $S_{s-n}(f) = 2\alpha^2 P_s N_{ASE}/N_{MM}$ within the detector electrical bandwidth B_e [28]. The photon count variance arising from $\alpha P_{s-n}(t)$ is given by

$$\sigma^2(K_{s-n}) = \overline{\left(\int_{-\Delta t/2}^{\Delta t/2} \alpha P_{s-n}(t)dt\right)^2} = \Delta t\int_{-\infty}^{\infty} \mathrm{Tri}(\frac{\xi}{\Delta t})\Gamma(\xi)d\xi = I_{s-n}\Delta t,$$
$$I_{s-n} \equiv \int_{-\infty}^{\infty} S_{s-n}(f)\,\mathrm{sinc}^2(f\Delta t)\Delta t df. \quad (40)$$

Here $\Gamma(\xi) \equiv \alpha^2\overline{P_{s-n}(t)P_{s-n}(t+\xi)}$ is the autocorrelation of $\alpha P_{s-n}(t)$ and $\mathrm{Tri}(x)$ the triangular function. I_{s-n} can be approximated by $S_{s-n}(0) = 2\alpha^2 P_s N_{ASE}/N_{MM}$ when $B_e \gg 1/\Delta t$. On the other hand, $P_{n-n}(t)$ produces a mean photon count $\overline{K_{n-n}} = \alpha(2N_{\mathrm{ASE}}B_o\Delta t)$ with a variance given by [29]

$$\sigma^2(K_{n-n}) = \overline{K_{n-n}}(F_e + \delta_c),$$
$$\delta_c = \overline{K_{n-n}}/(2B_o\Delta t N_{MM}) = \alpha N_{\mathrm{ASE}}/N_{MM}. \quad (41)$$

To measure E_s precisely, P_s needs to be as high as ~1 mW for a high signal to noise ratio. Such a high P_s is also accompanied by a significant N_{ASE}. As a result, the variance $\sigma^2(E_s')$ of E'_s arises predominately from the s-n beat term even though $P_{n-n}(t)$ of the ASE produces a

#162650 - $15.00 USD Received 14 Mar 2012; revised 25 May 2012; accepted 12 Jun 2012; published 26 Jun 2012

photon count variance in great excess of the Poisson value. From Eq. (40), $\sigma^2(E_s')$ is found to be $\sigma^2(E_s') \cong 2N_{ASE}E_s / N_{MM}$.

To account for the error $\delta E_s' \equiv E_s' - E_s$, we expand $1/E'_s$ in S_{NK3} (defined in section 6) as $1/E_s' \equiv (1/E_s)[1-\delta E_s'/E_s + (\delta E_s'/E_s)^2]$. Obviously, $\delta E_s'$ values among different pulses are uncorrelated. The additional bias and variance of $\Delta\tau_{SNK3}$ arising from $\delta E_s'$ are found to be

$$b_{\Delta\tau E} \equiv -\frac{N_{ASE}}{N_{MM}}\left(\frac{1}{E_{sav}^{on}} - \frac{1}{E_{sav}^{off}}\right)\left(2 - < W_{avn} >\right), \tag{42}$$

$$\sigma_{\Delta\tau E}^2 \equiv \frac{2N_{ASE}}{N_{MM}}\left(\frac{1}{E_{sav}^{on}} + \frac{1}{E_{sav}^{off}}\right) < W_{avn} >. \tag{43}$$

The additional variance $\sigma_{\Delta\tau E}^2$ also scales with $< W_{avn} > \sim 1/n$. In order to bound the corresponding RRE to $< 10^{-4}$ (assuming $\Delta\tau \sim 2$, $n = 1$ and $N_{MM} = 1$), the ratio N_{ASE}/E_{sav} needs to be kept below 10^{-8}. Consider a practical case where the seed laser oscillator is polarized with a peak power P_{seed} and pulsewidth $\Delta t = 1\,\mu$s at the input of a single mode preamplifier having a noise figure $N_F = 4$. N_{ASE} arises mainly from the ASE in the preamplifier that has an equivalent PSD of $h\nu N_F/2$ (in each polarization) at the input of the amplifier [28]. Using $N_{ASE}/E_{sav} \cong h\nu N_F/(2P_{seed}\Delta t)$, the minimum seed laser peak power P_{seed} at the input of the preamplifier is estimated to be -16 dBm, which can be easily satisfied. Similarly, the additional bias $b_{\Delta\tau E}$ can be neglected even when the online and offline pulse energies differ significantly. Consequently, both the bias $b_{\Delta\tau E}$ and variance $\sigma_{\Delta\tau E}^2$, arising from the laser-ASE beat noise, are neglected in the present model.

C. Noise from background solar radiation

At the lidar receiver, the ASE from the laser transmitter becomes negligible even compared to the weak background solar radiation that has a low optical power spectral density $2N_{bgd}$. Equations (40) and (41) can still be applied to the background sun light, provided that N_{MM} is interpreted as the number of the received speckles and N_{ASE} is replaced by N_{bgd}. Since $\alpha N_{bgd}/N_{MM} \ll 1$, K_{n-n} from the background sun light becomes a Poisson process (for F_e = 1). The s-n beat term variance $\sigma^2(K_{s-n}) = 2\alpha N_{bgd}\overline{K_s}/N_{MM}$ is much smaller than the signal shot noise $F_e\overline{K_s}$ and thus can be neglected. For the background sun light, the shot noise variance $\sigma^2(K_{n-n}) = F_e\overline{K_{n-n}}$ could be reduced to $\sigma^2(K_{s-n})$ if the optical filter bandwidth B_o could be reduced to $\alpha P_s/[(1+1/\beta)N_{MM}F_e]$. In practice, the optical filter bandwidth is much wider so that $\sigma^2(K_{n-n})$ is much larger than $\sigma^2(K_{s-n})$.

Acknowledgments

The authors gratefully acknowledge Dr. J. Mao and Dr. X. Sun of NASA Goddard for fruitful discussions and help in atmospheric modeling and lidar link budget calculations. They are also indebted to Dr. A. Amediek of Deutsches Zentrum für Luft- und Raumfahrt (DLR) for sharing surface reflectance measurement data, Dr. J. Abshire and other members of the Goddard CO_2 sounder team for their support. This work was supported by the NASA Goddard Internal Research and Development program and the NASA Earth Science Technology Office Instrument Incubator Program.

#162650 - $15.00 USD Received 14 Mar 2012; revised 25 May 2012; accepted 12 Jun 2012; published 26 Jun 2012